# Phase-Shift Depth Migration for qP and qSV wavefields on locally Transverse Isotropic Media

Marco Antonio Cetale Santos*, DEE/PUC-Rio, Djalma Manoel Soares Filho, PETROBRAS S/A Brazil , Paulo Léo Manassi Osório,DEE/PUC-Rio



## Abstract

Through numerical seismic data we investigate the robustness of pre-stack depth migration in relation to the symmetry axis variations on locally transverse isotropic (LTI) media. For modeling, we use a generalization of the finite differences scheme introduced by (Zahradník and Priolo, 1994) to accommodate seismic modeling on LTI media defined by six parameters at each grid point, i.e., density, P and S phase velocities along the local symmetry axis, the Thomsen parameters (Thomsen, 1986) and, the direction of the local symmetry axis itself. In relation to depth seismic imaging on LTI media, we generalize a method based on the phase-shift technique proposed by (Rousseau, 1997) to handle pre-stack depth migration for qP and qSV on such media. We carry out seismic modeling and pre-stack migrations by varying the direction of the local symmetry axis around its true value. The stability of the method is exhibited through qP and qSV migrations for one common shot gather.

## Introduction

Pre-stack depth migration (PSDM) applied to transverse isotropic media with a global vertical, or tilted, symmetry axis has been one of the most important subjects faced by geoscientists. In fact, there are a huge number of papers presenting effective strategies for depth imaging when this kind of anisotropy is involved, e.g., (Kitchenside, 1991), (Faria, 1993) and (Uzcategui, 1994). However, as (Thomsen, 2002) indicates on his Distinguished Lectures Notes, there are cases when the assumption of a unique vertical or tilted symmetry axis should not be applied (dipping polar anisotropic media). In other words, in these cases the local symmetry assumption, instead of the global one, is more realistic. In the present work, we consider modeling and depth-migration on LTI media to handle such cases.

For multi-component seismic modeling, we generalized the second order explicit finite differences scheme proposed by (Zahradník and Priolo, 1994) to take into account 2-D non-homogeneous LTI media, as it is briefly explained in this paper.

For seismic imaging, we generalize a phase-shift type algorithm, based on the one proposed by (Rousseau, 1997), to accommodate continuous changes of the symmetry axis along the model on qP and qSv pre-stack depth migration.

## Modeling for LTI Media

Given the Thomsen parameters ($\varepsilon$, $\delta$), P and S wave propagation velocities ($\alpha$, $\beta$), for each medium point, plus the density $\rho$, we can compute the elastic coefficient tensor in terms of the local coordinate system. According to (Thomsen, 2002), we apply a rotation matrix $R(\phi)$, where $\phi$ specify the local axis direction, given by:

$$R(\phi) = \begin{bmatrix} \cos\phi & 0 & -\sin\phi \\ 0 & 1 & 0 \\ \sin\phi & 0 & \cos\phi \end{bmatrix},$$

which transforms the elastic tensor coefficients, $c_{ijkl}$, into the global axis coordinates system:

$$c'_{IJKL} = R_{Ii}.R_{Jj}.R_{Kk}.R_{Ll}.c_{ijkl}\,.$$

In this way, the wave equation is solved using a generalization of the finite differences scheme proposed by (Zahradnik and Priolo, 1994):

$$\frac{\partial \Gamma_{ij}}{\partial x_i} + f_i = \rho \frac{\partial^2 u_i}{\partial t^2} \qquad \text{and} \qquad \Gamma_{ij} = c'_{ijkl} \cdot \partial u_k / \partial x_l$$

where $\Gamma_{ij}$ - stress tensor components, $u_i$ – displacement vector components $f_i$ – external force density.

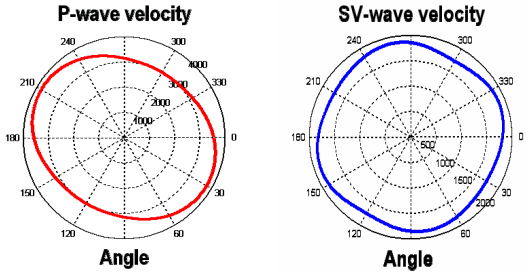


Figure 1 – P and SV phase velocities used to generate the snapshot in figure 2, for $\varepsilon$=0.3, $\delta$=0, and $\phi$=30°.

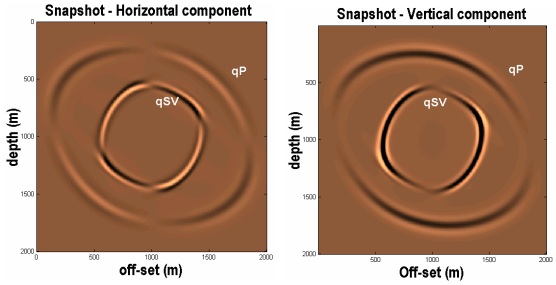


Figure 2 – Snapshot components for parameters defined in figure 1.

Figure 2 shows a snapshot generated by this algorithm for a homogeneous medium with phase velocities P and SV as shown in figure 1.

This method is presented in more detail in a companion paper submmited to this SBGf congress (Cetale Santos et al.,2003b).

**Phase-Shift PSDM for LTI Media**

In the pos-stack migration process we can use the scalar wave equation in the frequency domain, which solution is given by:

$$P(k_x, z_0 + \Delta z, \omega) = e^{ik_z \Delta z} P(k_x, z_0, \omega)\,. \qquad (1)$$

After applying a 2D inverse Fourier transform we get p*(x, z+Δz,t), as shown by* (Gazdag, 1974). For an upward solution, we use.

$$k_z = -\sqrt{\frac{w^2}{v^2} - k_x^{\,2}}\,, \qquad (2)$$

where $k_x$, $k_z$, $\omega$ and $v$ are the spatial frequencies, the temporal frequency and velocity, respectively.

In modeling, the solution in equation (1) only propagates waves from the reflectors up to the receivers, using a $\Delta z$ with a negative sign. In the migration case $\Delta z$ has a positive sign.

This methodology is applied in pos-stack migration, where half of the propagation velocity is employed in order to correct for the two way traveltime, and the image condition is given for t=0.

For pre-stack migrations, we depropagate each seismogram separately and use a different image condition from pos-stack migration which is given by the direct arrival traveltime at each medium point, i.e.,

$$P(k_x, z_0 + \Delta z, \omega) = e^{-i\omega . TD} e^{ik_z \Delta z} P(k_x, z_0, \omega) \qquad (3)$$

where *TD* denotes the direct arrival traveltime.

In this way, for the isotropic grid points, $k_z$ will be computed according to equation (2). On the other hand, for the LTI grid points, $k_z$ will be estimated by the following algorithm. In doing this, we created a hybrid method.

Given the dispersion relation:

$$\left(\frac{\omega}{v}\right)^2 = k_x^2 + k_z^2\,,$$

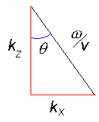


and taking into account the following trigonometric relations:

$$\frac{k_x}{\omega} = \frac{\sin\theta}{v(\theta - \phi)} \quad \text{and} \quad \frac{k_z}{\omega} = \frac{\cos\theta}{v(\theta - \phi)}\,,$$

the spatial frequency $k_z$ is estimated through a table generated by varying $\theta$ between 0 and $\pi$ rad, and by computing $\sin\theta / v(\theta-\phi)$ and $\cos\theta / v(\theta-\phi)$, which are related to the values of $k_x/\omega$ and $k_z/\omega$. Once we have the values of $k_x$ and $\omega$ it is possible to determine $k_z$ from the table. For some values of $k_x$ and $\omega$, $k_x/\omega$ is outside the $\sin\theta /v(\theta-\phi)$ table. Such values represent the horizontal slowness of the evanescent waves, i.e., $k_z$ is a imaginary number, and the wavefield is zeroed.

The P-P and P-SV wave migrations are computed using this hybrid algorithm, whose imaging conditions are given by the compressional direct arrival time as mentioned before.

We compute the phase velocities fields using the following (Thomsen, 1986):

$$v_P^2(\theta') = \alpha^2\left[1 + \varepsilon \cdot \sin^2(\theta') + D(\theta')\right] \quad \text{and}$$

$$v_{SV}^2(\theta') = \beta^2\left[1 + \frac{\alpha^2}{\beta^2}\varepsilon \cdot \sin^2(\theta') - \frac{\alpha^2}{\beta^2} D(\theta')\right]$$

where

$$D(\theta') = \frac{f}{2}.\left\{\left[1 + \frac{4\delta}{f^2}\sin^2\theta'\cos^2\theta' + 4\frac{(f+\varepsilon)}{f^2}\varepsilon\sin^4\theta'\right] - 1\right\},$$

$$f = 1 - \frac{\beta^2}{\alpha^2} \quad \text{and} \quad \theta' = \theta - \phi\,,$$

i. e., $\theta'$ is the angle between the normal to the wave front and the local symmetry axis.

In order to compute the compressional direct arrival traveltime, a technique similar to the hybrid method is employed. In this case, a downward modeling is implemented with an impulsive source located at the same position where the shot was generated in the LTI modeling.

**Examples**

For the modeling stage we use an explosive Ricker source where the cutoff frequency was limited to 60 Hz. This source is employed in order to generate only P waves, however the upper surface reflections also generate SV waves. To remove these wave-modes and the ones generated along the other frontiers, an absorbing boundary condition technique was employed. (Cerjan, et all,1986).

The S wave velocity was computed from the P wave velocity, using the Poisson coefficient of 1/4, and the grid was adequately discretized in order to avoid numerical dispersion and instabilities.

Instead of applying muting or f-k transform to remove the direct wave, a modeling of the first layer was used. We considered the difference between the complete seismogram and the direct wave one.

In the two models presented here, the first layer was made isotropic, which allowed the P and SV wavefields to be computed through the divergent and the rotational operators, respectively, as in (Sun, 1999). However, if these layers were anisotropic, then the propagated waves through this media would be qP and qSV, and the previous operators would be inefficient. In this case, the computation of the qP and qSV waves can be implemented with a technique proposed by (Dellinger, 1991).

The velocity fields $\alpha$ and $\beta$ were smoothed in order to guarantee that most of the energy will arrive at the deepest reflectors.

For transverse isotropic media a table is built for each medium, where the employed increment angle was 0.5°.

We performed seismic simulations on two different models. In Example 1 the model has three layers with flat interfaces as shown in figure 3-(a), where the main objective was to recover the interface at 1400 m. In this example the central layer is anisotropic with an inclination of $\phi$ =20° and $\varepsilon$ =0.3. In figure 2, we can observe the wave propagation in an anisotropic homogeneous medium with the same characteristics. The parameters for this model are on table 1. The PSDM is carried out for only one shot and for an explosive source located at the center of the model and at 12 m of depth. A 400x600 regular grid with 4 m interval was used.

Figures 3-(b) and (c) show the migration results using the same parameters used in the modeling, for the P and SV waves, respectively. We can observe from figure 3-(b) that most of the energy is concentrated to the right, which is the place where the phase shift occurs in figure 3-(c). If we take the wavelet peaks as a reference for the interface locations, we can see that they locate exactly the interfaces in both the P and SV waves images.

Figures 4-(a) and 5-(a) show the migration results for an isotropic processing, using $v_P=\alpha$ e $v_{SV}=\beta$ in the anisotropic layer. Figures 4 and 5, (b), (c), (d), (e) and (f) were obtained by the symmetry axis variations in the second layer. We can observe the changes in the interfaces positioning with different angles. In figure 4-(e) the positioning error is very large for the P wave image, and in figure 5-(e), besides the positioning error the interface appears tilted.

Tables 3 and 4 show the positioning errors for the interface located at 1400 m of depth, relative to the different migration models. They were obtained by the difference between the interface correct position and the largest wavelet peak in the migrated image. These errors were computed for 3 traces at 1100, 1200 (source location), and 1300 m. The results in table 4 were obtained with an isotropic processing. In the first test, the true vertical velocities were computed from the anisotropic parameters, whereas in the second test the $\alpha$ e $\beta$ velocities were employed.

In table 4, we have the results obtained by deviating the symmetry axis from the true one, and by considering the true values of $\alpha$, $\beta$, $\varepsilon$, $\delta$ and $\rho$. Some migrated sections are exhibited in figures 4 and 5.

It was shown in (Cetale Santos et. al, 2003a), that for small changes in the inclination angle of the symmetry axis, the error in the P wave image is small. In the present work, we also show that the same occurs with the SV wavemode. The changes in this angle result in different error variations in the P and SV images, as expected, since the P and SV velocity fields can have different forms. Figure 1 illustrates these variation forms for the P and SV wave phase velocities.

In example 2, we present the PSDM for the model shown in figure 6. A 400x800 regular grid with 4 m interval was used. We considered one common shot point gather, with the source located at the center of the model and at 12 m of depth. Figures 8-(a) e (b) show the results of the anisotropic PSDM, for P and SV waves, respectively. We can see that the interfaces were partially recovered with precision. In the case at the corresponding SV image, we can see a better resolution, as it was expected.

Figures 9-(a) and (b) exhibited the results of the isotropic PSDM using the $\alpha$ and $\beta$ velocities, respectively. Note that in the case of the P image, that there are small positioning errors in relation to the horizontal interface at 1360 m depth, which is not presented in the SV case. In reality, in this last case, there are errors but smaller than the former one.

| Medium | ρ | α | β | ε | δ | Dip ($\phi$) |
|---|---|---|---|---|---|---|
| 1 | 2460 | 2950 | 1703 | 0 | 0 | $0^0$ |
| 2 | 2460 | 3000 | 1732 | 0.3 | 0 | $20^0$ |
| 3 | 2460 | 3600 | 2079 | 0 | 0 | $0^0$ |

Table 1 – Thomsen parameters for example 1.

| Medium | ρ | α | β | ε | δ | Dip ($\phi$) |
|---|---|---|---|---|---|---|
| 1 | 2460 | 2500 | 1443 | 0 | 0 | $0^o$ |
| 2 | 2460 | 2550 | 1472 | 0.1 | 0 | $10^o$ |
| 3 | 2460 | 2700 | 1559 | 0.2 | 0.1 | $30^0$ |
| 4 | 2460 | 3000 | 1732 | 0.2 | 0.1 | $-10^0$ |
| 5 | 2460 | 3000 | 1732 | 0 | 0 | $0^o$ |
| 6 | 2460 | 3100 | 1790 | 0 | 0 | $0^o$ |
| 7 | 2460 | 3300 | 1905 | 0 | 0 | $0^o$ |
| 8 | 2460 | 3500 | 2021 | 0 | 0 | $0^o$ |

Table 2 – Thomsen parameters for example 2.

| | Reflector positioning error in (m) in the off-sets: | | | | | |
|---|---|---|---|---|---|---|
| Migration velocity | **P wave** | | | **SV wave** | | |
| | **1100 m** | **1200 m** | **1300m** | **1100 m** | **1200 m** | **1300 m** |
| $V_p(90°)$ and $V_{sv}(90°)$ | -4 | 0 | -4 | 0 | 0 | -4 |
| $\alpha$ and $\beta$ | -20 | -16 | -20 | -28 | -28 | -24 |

Table 3 – Isotropic migration positioning error.

| | Reflector positioning error in (m) in the off-sets: | | | | | |
|---|---|---|---|---|---|---|
| Migration axis inclination | **Wave P** | | | **Wave SV** | | |
| | 1100 m | 1200 m | 1300 m | 1100 m | 1200 m | 1300 m |
| 20º | 0 | 0 | 0 | 0 | 0 | 0 |
| 0° | -16 | -16 | -16 | -28 | -28 | -28 |
| 20º+5 | +16 | +12 | +12 | +12 | +12 | +16 |
| 20°+15° | +44 | +44 | +44 | +24 | +32 | +40 |
| 20°+25° | +80 | +80 | +80 | +32 | +46 | +60 |
| 20°+35° | +112 | +116 | +120 | +32 | +52 | +68 |
| 20°+45° | +140 | +148 | +148 | +32 | +52 | +68 |
| 20°+65° | +176 | +180 | +180 | +36 | +44 | +48 |
| 20°-5° | -8 | -8 | -8 | -8 | -8 | -12 |
| 20°-15° | -16 | -16 | -16 | -28 | -28 | -24 |
| 20°-25° | -16 | -16 | -16 | -28 | -24 | -28 |
| 20°-35° | -8 | -8 | -8 | -12 | -8 | -4 |
| 20°-45° | +12 | +12 | +16 | +16 | +16 | +16 |
| 20°-65° | +80 | +80 | +80 | +56 | +44 | +56 |

Table 4- Anisotropic Migration positioning error.

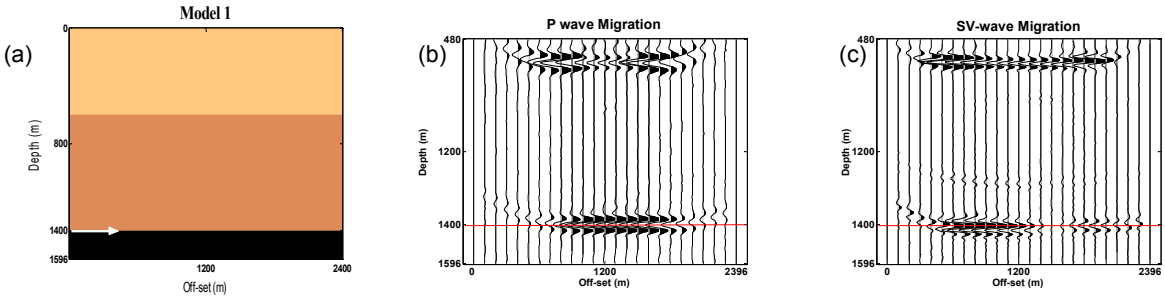


**Figure 3- (a) Model 1 (b) P-wave anisotropic migration (c) SV-wave anisotropic migration.**

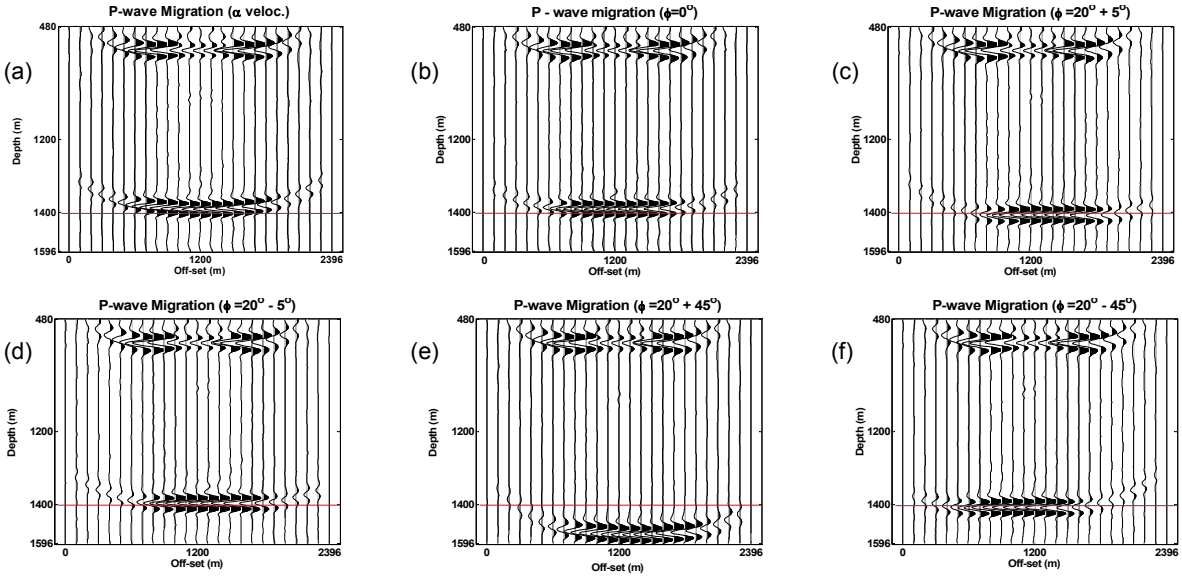


**Figure 4 – Model one P-wave migration with different parameters: (a) Isotropic layers with the respective $\alpha$ velocities, (b),(c),(d),(e) e (f) Different angles for layer 2: For $\phi$ = 0°,15°, 25°, 65° e -15°, respectively.**

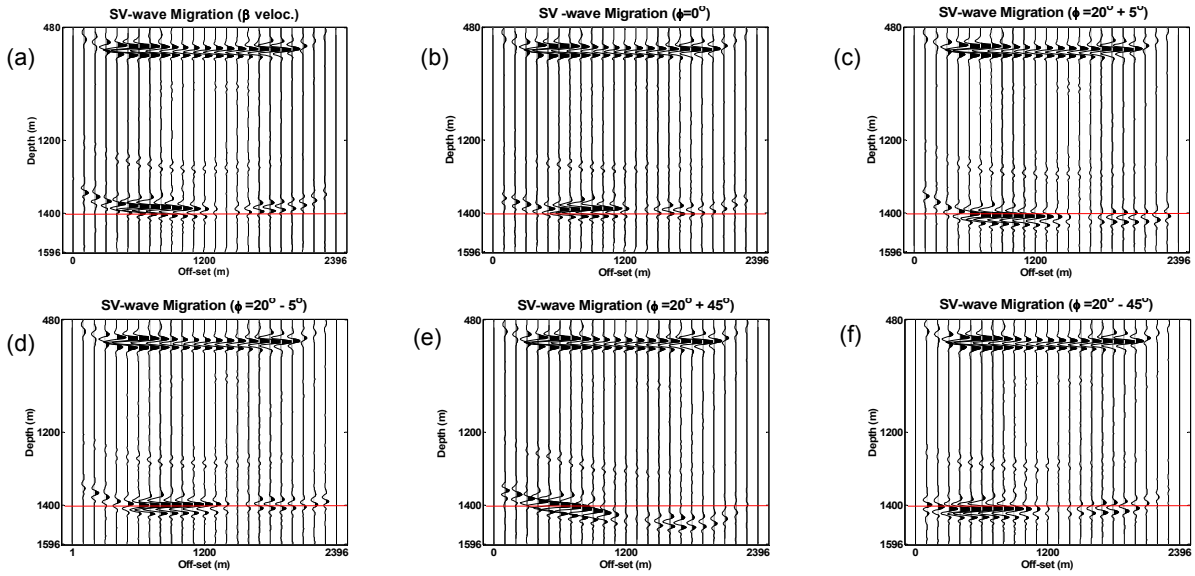


**Figure 5 – Model one SV-wave migration with different parameters: (a) Isotropic layers with the respective $\beta$ velocities, (b),(c),(d),(e) e (f) Different angles for layer 2: For $\phi$ = 0°,15°, 25°, 65° e -15°, respectively.**

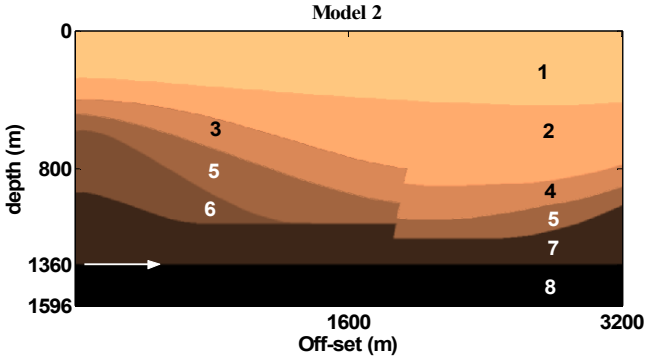


Figure 6- Synthetic model of Example 2.

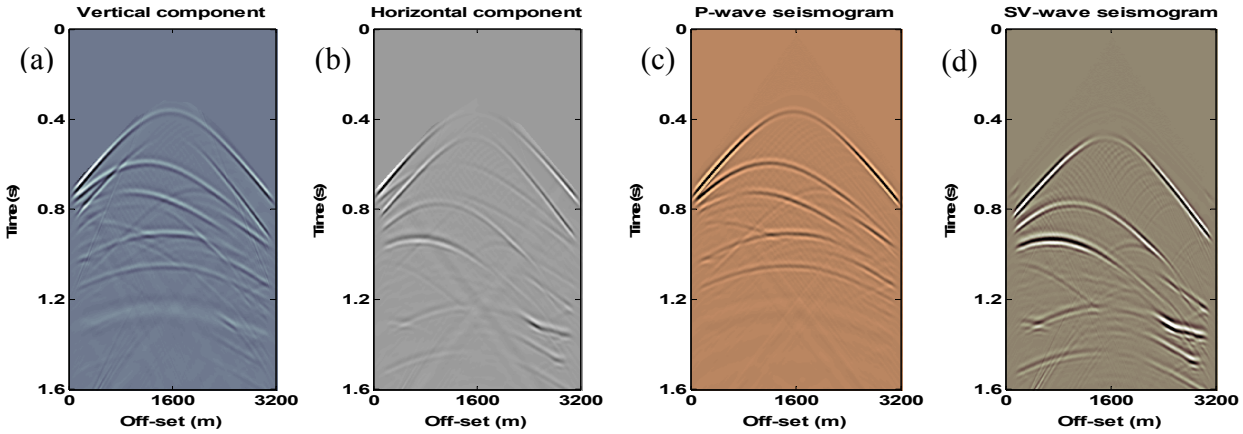


Figure 7- Seismograms: (a) vertical component, (b) Horizontal component, (c) P-wave, (d ) SV- wave.

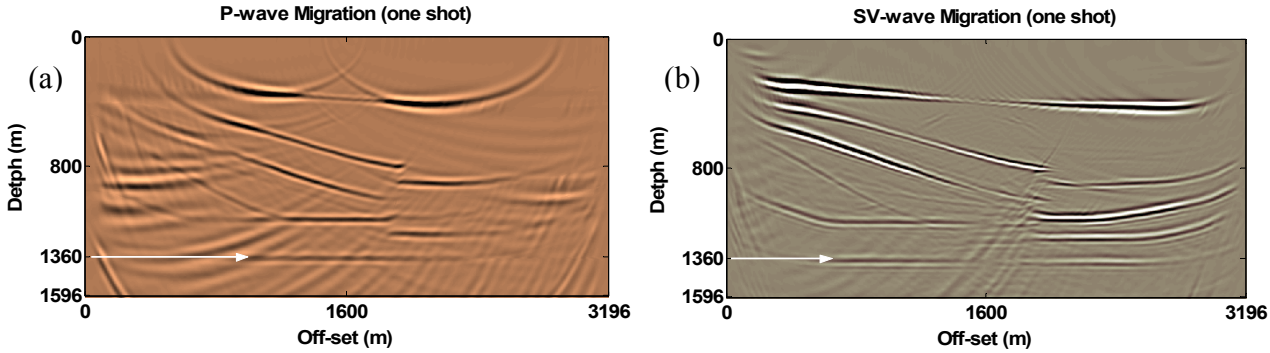


Figure 8 – Migration with modeling parameters (a) P-wave (b) SV-wave.

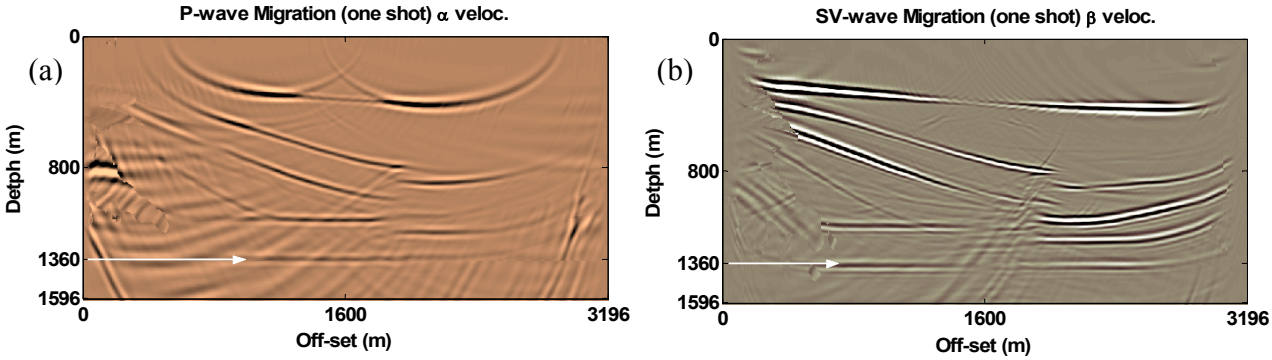


Figure 9 – Migration with isotropic parameters (a) α velocity for P-wave, (b) β velocity for SV-wave.

**Discussions of Results/Conclusions**

In the Example 1 the model presents a 0.8 km anisotropic layer with an extreme value for $\varepsilon$, according to table 1 in (Thomsen, 1986). When we use the true parameters as input to the PSDM, we precisely recover the reflector at 1400m depth, in both P and SV waves, as It can be seen in figure 3.

In order to stack the SV migrated images, the first step is to correct the SV wave phase. This correction is not trivial, since it gets worse with the anisotropy. To exemplify this fact, we can compare the example given in (Sun and Wang, 1999) with Example 1, in the present work. Both examples have two interfaces, but in the first one all the layers are isotropic. Since the layers are parallel, the SV wave phase shift for the isotropic media occurs exactly bellow the source trace position, and the author proposes a simple phase correction where he multiplies by -1 all the seismic traces to the left of the source position. Unfortunately, this procedure cannot be applied when anisotropy is involved. From figure 3-(c), we can see that for the first interface there is not an abrupt phase shift. For the second interface, the phase shift occurs to the right of the source location, in a position that depends on the inclination of the symmetry axis of the anisotropic layers.

In the Example 2 the model has more structural complexities. It includes a fault and three transversally isotropic layers with symmetry axes in three different directions. When we used the true parameters in the PSDM, the interfaces that were illuminated properly were successfully recovered, by using just one shot gather. Besides, we can also see a better resolution in SV wave image.

We also observed that in LTI media, the phase shifts can occur in the reflectors of the P-wave seismograms. This phenomenon is caused by the different incidence angles of the wave front with the interfaces. For an anisotropic interface (isotropic-anisotropic, anisotropic-isotropic or anisotropic-anisotropic layers), it means that for a given incidence angle the velocity relations between layers are different, which can cause velocity inversions. Figure 7-(c) shows a phase shift in the third reflector, this also appears in the respective images shown in figures 8-(a) and 9-(a).

Even though, the results presented here refer to P-P and P-SV waves, the proposed method is not restricted to these wave modes, i.e, migrations can be computed for the reflected waves SV-P and SV-SV, as well.

The method employed in this work is not restricted to multi-component surveys, even though we have dealt only with horizontal and vertical displacement wavefields.

Finally, we emphasize that our method does not involve any interpolation procedure to handle continuous changes of parameters along each horizontal level, as it is the case of Phase-Shift Plus Interpolation (PSPI) type techniques as in (Gazdag and Squazzerro, 1984). Instead we compute the wavefield at each point considering its local parameters. We adopt this procedure for two reasons: interpolation processes are not trivial when six parameters are involved, and the wavefield extrapolation can be accomplished in a high parallel fashion by exploring the complete independent characteristics of the proposed method.

**References**

**Cerjan, C., Kosloff, D. Kosloff, R. e Reshef, M.**, 1985, A nonreflecting boundary condition for discrete acoustic and elastic wave equations, Geophysics, 50, 705-708.

**Cetale Santos, M. A., Soares Filho, D. M. and Osório,P. L. M.**, 2003a, Phase-Shift Depth Migration on Locally Transverse Isotropic Media: Stability in Relation to Symmetry Axis Variation at Each Medium Point, Submitted to Soc. Expl. Geophys., Annual Meeting.

**Cetale Santos, M. A., Soares Filho, D. M., Osório, P. L. M. and Rosa Filho, J. C.**, 2003b, Modelagem sísmica em meios localmente Transversalmente Isotrópicos, Submitted to 8th International Congress of The Brazilian Geophysical Society.

**Dellinger, J.**, 1991, Anisotropic Seismic Wave Propagation, Ph. D. Thesis, Department of Geophysics of Stanford University.

**Faria, E. L. de**, 1993, Modeling, Migration and Focusing Analysis in Transversely Isotropic Media. Ph. D. thesis. The University Texas at Austin.

**Gazdag, J. and Sguazzero, P.**, 1984, Migration of seismic data by phase shift plus interpolation: Geophysics, 49, 124-131.

**Kitchenside, P. W.**, 1991, Phase shift-based migration for transverse isotropy. 61st Annual Internat. Mtg., Soc. Expl. Geophys., Expanded Abstract.

**Rousseau, J. H. Le**, 1997, Depth migration in heterogeneous, transversely isotropic media with the phase-shift-plus-interpolation method: CWP-249, Colorado Scholl of Mines.

**Sun, R. and Wang, A.**, 1999, Scalar reverse-time depth migration of pre-stack elastic seismic data, 69th Annual Internat. Mtg., Soc. Expl. Geophys., Expanded Abstracts.

**Thomsen, L.**, 1986, Weak elastic anisotropy: Geophysics, 51, 1954-1966.

**Thomsen, L.**, 2002, Understanding Seismic Anisotropy in Exploration and Exploitation, Distinguished Instructor Series, No. 5., SEG and EAGE.

**Uzcategui, O**., 1994, Depth Migration in Transversely Isotropic Media with Explicit Extrapolators. Ph.D. thesis, Center for Wave Phenomena, Colorado School of Mines, Golden, Colorado 80401-1887. CWP-163.

**Zahradník, J. and Priolo, E**., 1994, Heterogeneous formulations of electrodynamics equations and finite-difference schemes, Seismic waves in complex 3-d structures, Report 1, Dept. of Geoph., Charles University.

**Acknowledgments**

The authors would like to thank PETROBRAS for the financial support though the PRAVAP 19 research program. To the Brazilian Research Council (CNPq) for the support though a doctor scholarship for the first author.